# Comparative analysis of temperature and $CO_2$ fluxes for winter wheat in Tibetan Plain and North China Plain using the EMD method*

JIANG Zhaoyang[1,2], YU Qiang[2**], LEI Shuhe[3], WANG Tianduo[4], SUN Xiaomin[2] and ZHANG Renhua[2]

(1. Chinese Academy of Meteorological Science, Beijing 100081, China; 2. Institute of Geographic Sciences and Natural Resources Research, Chinese Academy of Sciences, Beijing 100101, China; 3. Mathematics Department, Ocean University of China, Qingdao 266071, China; 4. Shanghai Institute of Plant Physiology and Ecology, Chinese Academy of Sciences, Shanghai 200032, China)

Received January 10, 2006; revised April 7, 2006

**Abstract** Comparative study of spectral properties of temperature and $CO_2$ fluxes measured by eddy covariance method at Yucheng (36°57′N, 116°36′E, 28 m a.s.l., in the North China Plain) and at Lhasa (29°41′N, 91°20′E, 3688 m a.s.l., on the Tibetan Plateau) is described using the empirical mode decomposition (EMD) method. The main results are: (1) The intrinsic oscillation modes or intrinsic mode functions (IMFs) were extracted from data of temperature ($T$) and $CO_2$ fluxes ($F$) measured at Yucheng ($T_1$ and $F_1$) and Lhasa ($T_2$ and $F_2$). (2) Hilbert transform was applied to these IMF components, then the Hilbert-Huang spectra and the marginal spectra of these data were obtained. (3) Comparison of temperature and $CO_2$ fluxes in North China Plain and on Tibetan Plain illustrated that the characteristic frequencies corresponding to $T_1$, $F_1$, $T_2$ and $F_2$ are 0.05 Hz, 0.03 Hz, 0.014 Hz and 0.005 Hz, respectively.

**Keywords:** **empirical mode decomposition (EMD), intrinsic mode function (IMF), flux, Hilbert transform, wheat, Tibet.**

Microclimatic variables like temperature and $CO_2$ flux are non-linear and non-stationary stochastic variables[1,2]. A series of continuous records of these variables often contain components with time scales from seconds to months[3,4]. Changes in temperature and flux density are the results of variations of microclimatic factors and characteristics of plants, caused by interactions between atmospheric movements and physiological processes of vegetation[5,6]. The analysis of spectral properties of variations with time series of microclimatic variables may help to reveal the causes of the changes in density and frequency of the variables[7—9]. Many models developed to describe the interactions between the biosphere and atmosphere have become essential parts of simulations of regional or global climatic processes[10—12]. This multi-scale nature of microclimatic variables is now being simulated by some models using data of long-term (over one or more years) measurement[13], but periods shorter than a day do not appear in the results of such simulations[14].

Spectral and auto-correlation or cross-correlation analyse are often used in meteorology[15,16] with some success. The traditional method used in spectral analysis is Fourier transform, which has been used successfully in the analysis of time series of land surface fluxes.[17] However, as has been pointed out by some authors[18,19], Fourier transform finds only limited use in the analysis of non-stationary signals, which has many components of different frequencies. To extract information from such signals, it is desirable to use windows with different temporal characteristics so that both high-frequency information with high precision and wholesome low-frequency information can be obtained[20]. Signal decomposition can be implemented in many ways, for instance, by some set of appropriate eigenfunctions[21,22]. Recently, the wavelet eigenfunctions set has been of much use because it decomposes a signal into a convenient set of levels of resolution[23—25]. Unfortunately, in the case of non-stationary or non-linear signals, a large number of terms are needed for convergence which results in undesired spread of the signal energy among the various expansion modes[25]. To avoid this shortcoming, empirical mode decomposition (EMD) method has been devel-

* Supported by the National Program on Key Basic Research Projects (Grant No. G1999-11708) and National Natural Science Foundation of China (Grant No. 40328001)

** To whom correspondence should be addressed. E-mail: zyjang@cams.cma.gov.cn

oped to analyze the non-stationary or non-linear signals[22,26]. The EMD method is included in the so-called Hilbert-Huang technique based on the direct extraction of the energy associated with the intrinsic time scales in the signal[22,26]. This process generates a set of components, called the intrinsic mode functions (IMF).

Tibetan Plateau is the highest plateau on the earth, which covers 1.2 million $km^2$ of area with an average height of more than 4000 m above sea level[27]. Because of its high altitude, it has the highest solar radiation (total radiation between 6704—7500 $MJ \cdot m^{-2} \cdot a^{-1}$) and lowest $CO_2$ partial pressure of all crop-growing regions on the Earth. It has been observed that global solar radiation even exceeded the solar constant on the plateau if the sky is clear and accompanied by some low clouds[28]. As solar radiation is the energy and $CO_2$ is one of the chief materials for photosynthesis, these influences on photosynthesis result in the fact that the productivity of vegetation is very different from that on low plains.

The aim of this study was to compare the spectral properties of temperature and $CO_2$ fluxes measured on Tibetan Plateau and in North China Plain using EMD method and Hilbert-Huang transform. Comparative analysis was adopted to reveal the changes in temperature and $CO_2$ fluxes measured in different areas on time scales from seconds to minutes, which may serve as the basis of building up models for microclimate of a particular locality and be more accurate and closer to reality.

## 1 Site description and experiment

Eddy covariance and meteorological measurements for winter wheat were carried out in 1994 at Lhasa Agricultural Experiment Station, Chinese Academy of Sciences (29°41′N, 91°20′E, 3688 m a.s.l.), on the Tibetan Plateau from June 10 to 30 under the extreme conditions of the highest solar radiation and lowest $CO_2$ partial pressure on the Earth. Similar measurements were also carried out in a low plain at Yucheng Agricultural Experiment Station, Chinese Academy of Sciences (36°57′N, 116°36′E, 28 m a.s.l.) in the North China Plain in 2002 from November 10 to 30. Yucheng belongs to the semi-arid temperate plateau climate zone. The fields in which measurements were performed occupied an area of 800 m × 1000 m and the fetch was more than 500 m for winds from all directions. During the period of measurements, the leaf area index (LAI) and the height of wheat canopy were 3.0 and 0.1 m, respectively.

The contents of observation include (1) microclimatic variables: solar radiation, net radiation at a reference height of 1 m, air temperature, relative humidity and wind speed at three heights (0.9, 1.77 and 3.37 m); (2) mass fluxes of $CO_2$ and water vapor between winter wheat field and the atmosphere measured by eddy covariance method.

The eddy-covariance measuring system comprised a $CO_2/H_2O$ infrared gas analyzer (Li-7500, LI-COR, USA, the sampling frequency is 20 Hz), and a triaxial sonic anemometer (DA600, KAIJO, Japan) set at a height of 2 m above the ground surface. A data taker sampled the data of all these variables every 20 Hz (Lhasa) and 10 Hz (Yucheng). These original data were then averaged every 1 s using the procedures described by Katul et al.[29—31].

## 2 Results and discussion

When examining the spectral properties of meteorological variables, it is helpful to consider three basic time scales: seconds to minutes (turbulent time scales), hours to days (meteorological time scales), and months to years (seasonal time scales)[9]. On the seconds to minutes time scales, the interactions between the physiological and biophysical processes of the canopy and its microclimate were driven mainly by atmospheric turbulence. The analysis is therefore focused on turbulent time scales, to compare the spectral properties of temperature and $CO_2$ fluxes measured in the North China Plain and Tibetan Plateau.

### 2.1 Data description

Eddy covariance measurements were carried out in the fields of winter wheat in1994 at Lhasa on the Tibtan Plateau, and in 2002 at Yucheng in the North China Plain. Time series of the 1s-averaged temperature and $CO_2$ flux measured from 11:00 to 12:00 on June 15, 1994 at Lhasa and on November 17, 2002 at Yucheng (a total of 3600 sets of data of each measurement) are shown in Fig. 1. The temperature ($T_1$) and $CO_2$ flux ($F_1$) measured at Yucheng are shown in Figs. 1(a) and (b), and the corresponding $T_2$ and $F_2$ measured at Lhasa are shown in Figs. 1(c) and (d). The time series of the four measurements are non-linear and non-stationary stochastic variables. There are rich pulsations superimposed on these measurements.

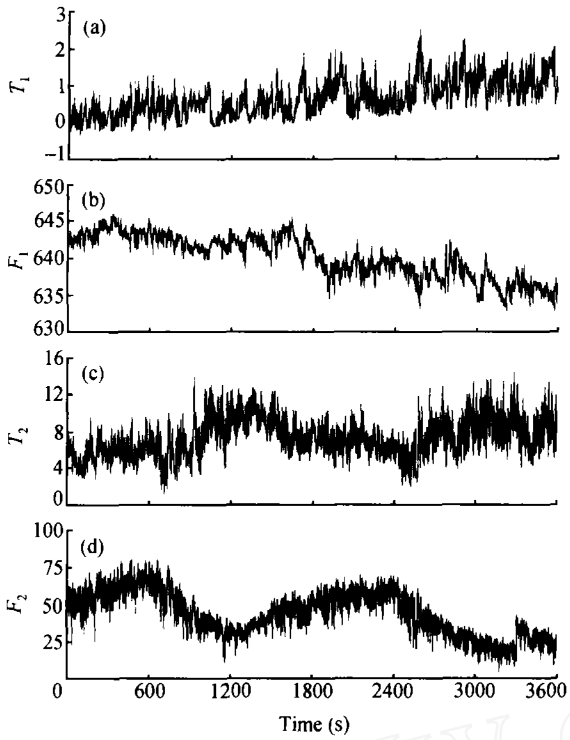


Fig. 1. Time series of temperature and $CO_2$ fluxes measured by eddy-covariance at 2 m above the ground surface at Yucheng and Lhasa (sampling frequency, $f_e = 1$ Hz). (a) Temperature measured at Yucheng ($T_1$); (b) $CO_2$ flux measured at Yucheng ($F_1$); (c) temperature measured at Lhasa ($T_2$); (d) $CO_2$ flux measured at Lhasa ($F_2$).

### 2.2 Application of empirical mode decomposition (EMD) to the extraction of the intrinsic mode functions (IMFs)

The intrinsic mode function (IMF) $c_i(t)$ represents the oscillation mode embedded in the data of temperature and $CO_2$ fluxes measured at Yucheng and Lhasa. Therefore, the decomposition of these time series expressed as IMFs will have two advantages. The first one is that it will allow us to examine the physical meaning of each IMF component. The second one is that the residual will contain the data trend, and in this way we can perform the analysis even if the data are not stationary.

The EMD method was applied to the analyses of the temperature and $CO_2$ fluxes shown in Fig. 1. There were a total of eleven IMFs components decomposed from the time series of $T_1$, $F_1$ and $F_2$, but the decomposition of the time series of $T_2$ gave a total of twelve IMFs components. The first four IMFs components $c_1$ to $c_4$ are probably associated with noise. $c_5$ to $c_8$, or $c_9$ components represent the main oscillation mode of the four measurements. The other components or low frequency components are related chiefly to the trend of the data.

### 2.3 Hilbert-Huang spectrum

Since the Hilbert-Huang transform defines the instantaneous frequency of each IMF, the transform was applied to the IMF matrix of the four measurements of $T_1$, $F_1$, $T_2$ and $F_2$. Then, the instantaneous frequency (IF), the average instantaneous frequency (AIF) and marginal Hilbert spectra could be calculated.

2.3.1 The Hilbert-Huang spectra of the data measured at Yucheng and Lhasa Fig. 2 shows the low-frequency domains (lower than 0.2 Hz) of the Hilbert-Huang spectra of $T_1$(a), $F_1$(b), $T_2$(c) and $F_2$(d). In all these figures displaying Hilbert-Huang spectra, the basic units are 1 s for time ($X$-axis) and 1 Hz for frequency ($Y$-axis), and the lighter the gray scales, the larger the values of the Hilbert-Huang transform coefficient. In the Hilbert-Huang spectra of the four measurements, most of the signal energy along the time axis accumulates from 0.03 Hz to 0.01 Hz and from 0.015 Hz to 0.005 Hz for $T_1$(a), from 0.02 Hz to 0.01 Hz and from 0.015 Hz to 0.004 Hz for $F_1$(b), from 0.015 to 0.01 Hz and from 0.008 to 0.003 Hz for $T_2$(c) and from 0.025 to 0.015 Hz and lower than 0.005 Hz for $F_2$(d), respectively. There are almost no energy concentrations in the domains lower than 0.005 Hz of the Hilber-Huang spectra of the data measured at Yucheng, but the domains concentrate most of the energy of the Hilbert-Huang spectra of the data measured at Lhasa on the Tibetan Plateau.

From the Hilbert-Huang transform, the average instantaneous frequency (AIF) of each IMF component of the four measurements was calculated. The AIFs of each IMF component of $T_1$, $F_1$, $T_2$ and $F_2$ are shown in Fig. 3. Almost each AIF of the IMF components $T_2$ and $F_2$ is slightly larger than these of $T_1$ and $F_1$.

2.3.2 The marginal frequency spectra of the data measured at Yucheng and Lhasa With the help of the sifting algorithm explained in Ref. [22], the marginal frequency spectra $h(\omega)$ can be deduced from the Hilbert-Huang spectra of the four measurements. Fig. 4 displays the marginal frequency spectra of $T_1$(a), $F_1$(b), $T_2$(c) and $F_2$(d). These marginal frequency spectra display very similar spectral properties to the Fourier spectra of these measurements, and the slopes of the spectra of $T_1$, $F_1$ and $T_2$ are nearly $-4/3$, but the slope of the spectrum of $F_2$ is nearly $-1$.

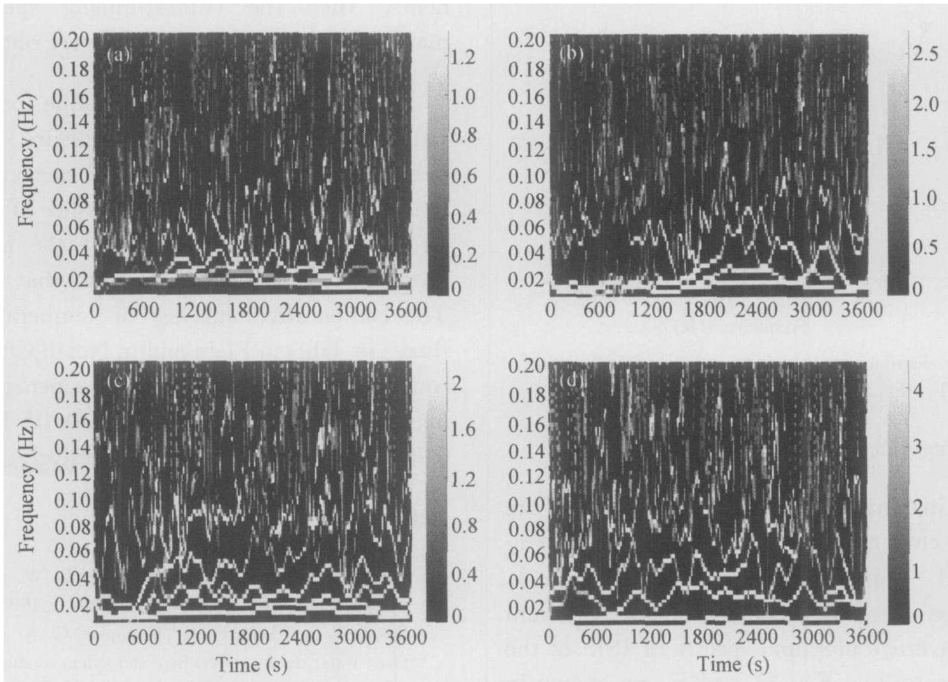


Fig. 2. Lower frequency domain (lower than 0.2 Hz) of Hilbert-Huang spectra $H(\omega, t)$ of $T_1$(a), $F_1$(b), $T_2$(c) and $F_2$(d).

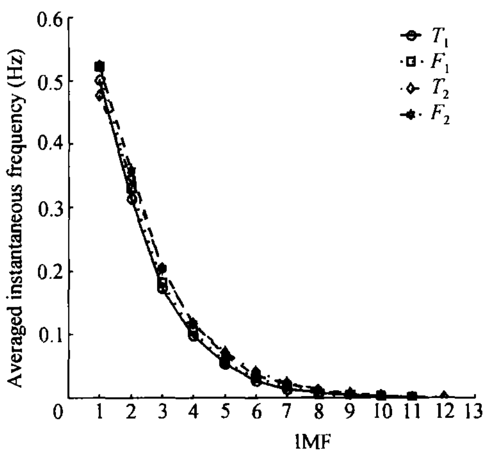


Fig. 3. The averaged instantaneous frequency (AIF) for IMFs of $T_1$, $F_1$, $T_2$ and $F_2$.

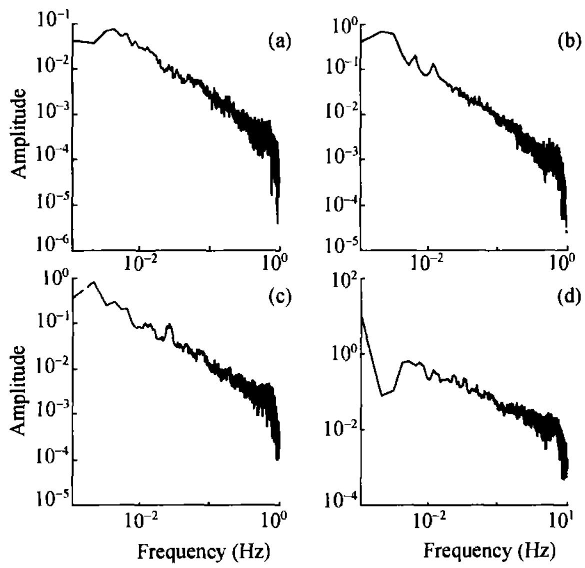


Fig. 4. The marginal spectra $h(\omega)$ of $T_1$(a), $F_1$(b), $T_2$(c) and $F_2$(d).

The percentages of relative energy accumulated at different frequency levels of resolution of the four measurements are presented in Fig. 5, which shows the energy distribution corresponding to the Hilbert-Huang spectra in Fig. 2. In Fig. 5, more than 60% of the energy (or amplitude) of the spectra of the four measurements are concentrated in the lowest frequency domain.

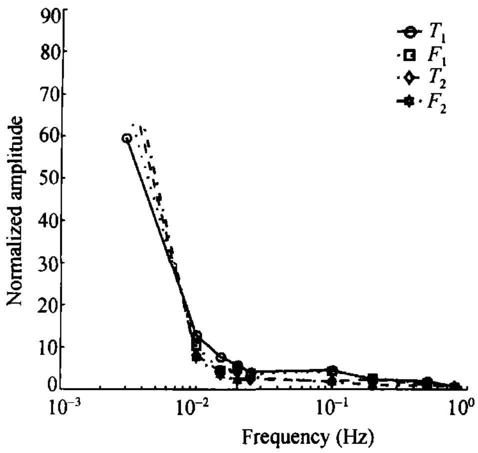


Fig. 5. Energy distribution plot corresponding to the marginal spectra $h(\omega)$ of $T_1$, $F_1$, $T_2$ and $F_2$.

### 2.4 The average local marginal spectra analysis

After the instantaneous frequencies of IMFs are computed, the characteristic frequencies located at $c_i$ can be obtained. The local marginal spectra $h'(\omega)_i$ can be obtained from the Hilbert-Huang spectrum analysis. The average marginal spectra of IMF of the four measurements $T_1$, $F_1$, $T_2$ and $F_2$ are shown in Fig. 6. The average marginal spectra illustrate clearly the characteristic frequencies corresponding to $c_8$(0.05 Hz) for $T_1$, $c_9$ for $F_1$(0.03 Hz), $c_{11}$ for $T_2$(0.014 Hz), and $c_{11}$ for $F_2$(0.005 Hz).

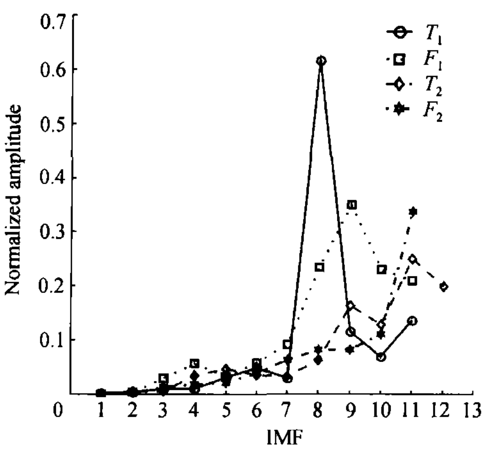


Fig. 6. Average marginal spectra of $T_1$, $F_1$, $T_2$ and $F_2$.

## 3 Conclusions

The EMD method has been shown to be a useful tool to analyze changes in micrometeorological variables in this study. The intrinsic oscillation modes or intrinsic mode functions (IMFs) were extracted from the data of temperature and $CO_2$ fluxes measured at Yucheng and Lhasa. The IMFs corresponding to low frequency (lower than 0.02 Hz) components were shown to be the main components for those variables. Hilbert transform was applied to these IMF components, then the Hilbert-Huang spectra and the marginal spectra of these data were obtained.

The climate in Tibet is unique for its high solar radiation and low $CO_2$ partial pressure. As solar radiation and $CO_2$ supply energy and carbon for photosynthesis, respectively, the importance of their influence on photosynthesis and thereby the productivity of vegetation is very different from that in low plains. The comparative analysis of temperature and $CO_2$ fluxes in Tibetan Plain and in North China Plain illustrated that the characteristic frequencies corresponding to $T_1$, $F_1$, $T_2$ and $F_2$ are 0.05 Hz, 0.03 Hz, 0.014 Hz and 0.005 Hz, respectively.

## References


1 Hutjes R. W. A., Kabat P., Running S. W. et al. Biospheric aspects of the hydrologic cycle. J. Hydrol., 1998, 213: 1—21.

2 Sperry J. S., Adler F. R., Campbell G. S. et al. Limitation of plant water use by rhizosphere and xylem conductance: results from a model. Plant, Cell, Environ, 1998, 21: 347—359.

3 Stull R. B. An Introduction to Boundary Layer Meteorology. New York: Kluwer Academic Publishers, 1988, 267—313.

4 Novak M. D., Wenjun C., Orchansky A. L. et al. Turbulent exchange processes within and above a strew mulch. Part I: Mean wind speed and turbulent statistic. Agric. For. Meteorol., 2000, 102: 139—154.

5 Cowan I. R. Transport of water in the soil-plant-atmosphere system. J. Appl. Ecol., 1965, 2: 221—239.

6 Lee X., Black T. A., den Hartog G. et al. Carbon dioxide exchange and nocturnal processes over a mixed deciduous forest. Agric. For. Meteorol., 1996, 81: 13—29.

7 Wilson J. D., Flesch T. K. and Harper L. A. Micro-meteological methods for estimating surface exchange with a disturbed wind flow. Agric. For. Meteorol., 2001, 107: 207—225.

8 Baldocchi D., Falge E. and Wilson K. A spectral analysis of biosphere-atmosphere trace gas flux densities and meteorological variables across hour to year time scales. Agric. For. Meteorol., 2001, 107: 1—27.

9 Katul G., Lai C. T., Schafer K. et al. Multiscale analysis of vegetation surface fluxes: from seconds to years. Adv. Water Res., 2001, 24: 1119—1132.

10 Goudriaan J. and van Laar H. H. Relations between leaf resistance, $CO_2$-concentration and $CO_2$ assimilation in maize, beans, lalang grass and sunflower. Photosynthetica, 1978, 12: 241—249.

11 Collatz G. J., Ball J. T., Grivet C. et al. Physiological and environmental regulation of stomatal conductance, photosynthesis and transpiration: A model that includes a laminar boundary layer. Agric. For. Meteorol., 1991, 54: 107—136.

12 Wang Y. P. and Leuning R. A two-leaf model for canopy conductance, photosynthesis and partitioning of available energy I: Model description and comparison with a multi-layered model. Agric. For. Meteorol., 1998, 91: 89—111.

13 Baldocchi D. and Wilson K. B. Modeling $CO_2$ and water vapor exchange in a temperate broadleaved forest across hourly to decadal time scales. Ecol. Model., 2001, 142: 155—184.

14 Yu Q., Goudriaan J. and Wang T. D. Modelling diurnal courses of photosynthesis and transpiration of leaves on the basis of stomatal and non-stomatal responses, including photoinhibition. Photosynthetica, 2001, 39: 43—51.

15 Baldocchi D. D. and Harley P. C. Scaling carbon dioxide and water vapor exchange from leaf canopy in a deciduous forest. II. Model testing and application. Plant Cell Environ., 1995, 18: 1157—1173.

16 Baldocchi D. and Meyers T. P. A spectral and lag-correlation analysis of turbulence in a deciduous forest canopy. Bound. Layer Meteorol., 1998, 45: 31—58.

17 Labat D., Ababou R. and Mangin A. Rainfall-runoff relations for Karstic springs. Part II: continuous wavelet and discrete orthogonal multiresolution analyses. J. Hydrol., 2000, 238: 149—178.

18 Mallat S. Image retrieval using wavelet-based salient points. Trans. Pattern Anal. Mach. Intell., IEEE., 1989, 11(7): 674—693.

19 Aballe A., Bethencourt M., Botana F. J. et al. Using wavelets transform in the analysis of electrochemical noise data. Electrochim. Acta, 1999, 44: 4805—4816.

20 Jordan D. A., Hajj M. R., Tieleman H. W. et al. Characterization of turbulence scales in the atmospheric surface layer with the continuous wavelet transform. J. Wind Eng. Indust. Aerodyn., 1997, 69—71: 709—716.

21 Huang N. E., Shen Z. and Long S. R. A new view of nonlinear water waves: the Hilbert spectrum. Annual Review of Fluid Mechanics, 1999, 31: 417—457.

22 Huang N. E., Shen Z., Long S. R. et al. The empirical mode decomposition and the Hilbert spectrum for nonlinear and non-stationary time series analysis. Proc. R. Soc. Lond., 1998, A (454): 903—995.

23 Roques S. and Meyer Y. Progress in wavelet analysis and applications. In: Proceedings of the International Conference "Wavelets and Applications", 1993, 758—759.

24 Foufoula-Georgious E. and Kumar P. Wavelet in Geophysics. New York: Academic Press, 1995, 373—343.

25 Jiang Z. Y., Yu Q., Wang T. D. et al. Continuous wavelet transform and discrete multi-resolution analysis of surface fluxes and atmospheric stability. Pro. Natural Soc., 2006, 16(4): 89—96.

26 Montesinos M. E., Muñoz-Cobo J. L. and Pérez C. Hilbert-Huang analysis of BWR neutron detector signals: application to DR calculation and to corrupted signal analysis. Annals of Nuclear Energy, 2003, 30: 15—727.

27 Li W. H. and Zhou X. M. Ecosystems of Qinghai-Xizang (Tibetan) Plateau and Approach to Their Sustainable Management (in Chinese). Guangzhou: Guangdong Science and Technology Press, 1998, 56—101.

28 Xie X. Q. Some characteristics of radiation fields on Tibetan Plateau in summer. Chin. Sci. Bull., 1983, 28: 426—429.

29 Katul G., Oren R., Ellsworth D. et al. A Lagrangian dispersion model for predicting $CO_2$ sources, sinks, and fluxes in a uniform loblolly pine (Pinus taeda L.) stand. J. Geophys. Res., 1997a, 102: 9309—9321.

30 Katul G., Parlange M. B., Kuhn G. et al. The turbulent eddy motion at the forest-atmosphere. J. Geophys. Res., 1997b, 102: 13409—13421.

31 Katul G., Hsieh C. I., Bowling D. et al. Spatial variability of turbulent fluxes in the roughness sublayer of an even-aged pine forest. Bound. Layer Meteorol., 1999, 93: 1—28.